ANNUAL REVIEWS

Annual Review of Marine Science

Beryllium Isotopes in Marine Science: Understanding Ocean Current and Ice Dynamics

Yusuke Yokoyama[1] and Adam D. Sproson[2]

[1]Atmosphere and Ocean Research Institute, The University of Tokyo, Kashiwa, Japan; email: yokoyama@aori.u-tokyo.ac.jp

[2]National Oceanography Centre, Southampton, United Kingdom

Annu. Rev. Mar. Sci. 2026. 18:121–39

First published as a Review in Advance on July 31, 2025

The *Annual Review of Marine Science* is online at marine.annualreviews.org

https://doi.org/10.1146/annurev-marine-040224-033226

Keywords

cosmogenic nuclides, ice sheet, weathering, ocean circulation, continental shelf, estuary, scavenging, beryllium

Abstract

The Earth's climate has been kept under Goldilocks conditions because a variety of feedback systems maintain the atmospheric pCO_2 within a narrow range. The ocean, as a large reservoir of carbon compared with the atmosphere, plays a key role in the climate system, and studying ocean process can help us better understand this system. Cosmogenic nuclides produced in the atmosphere and their ratio to a terrestrial counterpart can provide detailed depictions of Earth surface process, and they have therefore been utilized widely since it became possible to measure them with accelerator mass spectrometry. Beryllium isotopes ($^{10}Be/^{9}Be$) are one of the most useful isotope systems for this purpose. In this article, we summarize recent developments in beryllium isotope chemistry and the isotopes' relation to ocean current and ice sheet dynamics as well as weathering in relation to long-term climate.

1. INTRODUCTION

The Earth's carbon cycle is in balance due to carbon exchange between different reservoirs (Müller et al. 2022). Ocean chemistry regulates atmospheric pCO_2, which is controlled by the influx of terrigenous material via erosion and weathering induced by orogenic changes, glacial activity, and precipitation (Foster & Rohling 2013). Changes of even a few percent in these feedback mechanisms—such as increasing input of CO_2 from volcanism (e.g., Lee et al. 2013) or increasing chemical weathering (e.g., Jagoutz et al. 2016)—can dramatically alter climate (Foster et al. 2017). Continuous records obtained from marine sediments to monitor Earth surface processes are therefore a key to understanding the climate system.

Nuclides produced in the atmosphere provide useful tracers of Earth system processes. The Earth's surface is bombarded by high-energy cosmic rays that interact with elements in the upper atmosphere to produce cosmogenic nuclides, including radiocarbon (^{14}C), which is then oxidized to CO_2 and distributed to various reservoirs (Larsen et al. 2018). Among these nuclides, the cosmogenic isotope ^{10}Be is produced by spallation of oxygen and nitrogen in the atmosphere (also known as meteoric Be) and makes its way to the Earth's surface via wet and dry deposition (Lal & Peters 1967) (**Figure 1**). The production rate of meteoric ^{10}Be is modulated by solar activity and the geomagnetic field (e.g., Henken-Mellies et al. 1990; Robinson et al. 1995; Carcaillet et al. 2003, 2004; Knudsen et al. 2008; Ménabréaz et al. 2011; Sakuramoto et al. 2017; Simon et al. 2017, 2020), but due to a well-mixed stratosphere, the ^{10}Be deposition flux is controlled mainly by stratosphere/troposphere air exchange and the precipitation rate, leading to a higher flux at the midlatitudes and along storm tracks (Field et al. 2006, Heikkilä et al. 2009, Heikkilä et al. 2013). In arid regions, such as Antarctica, dry deposition starts to dominate, leading to significant ^{10}Be flux

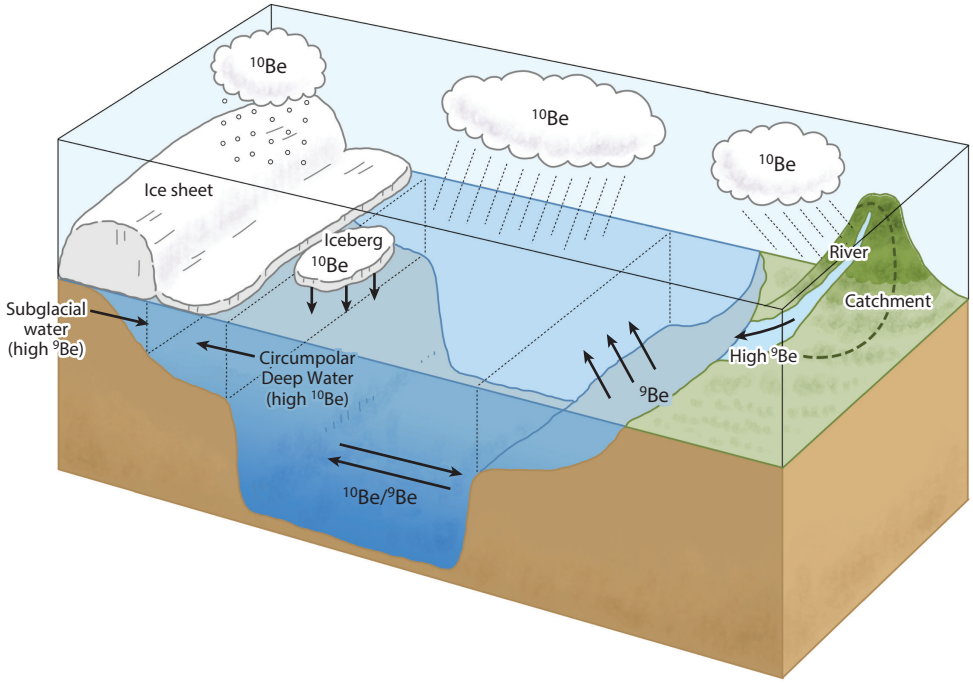

Figure 1

Schematic diagram of Be isotope distribution on the Earth's surface.

(Heikkilä et al. 2013). The stable isotope ^{9}Be is released during chemical silicate weathering and is transported to the ocean via rivers or aeolian dust (von Blanckenburg & Bouchez 2014, Suhrhoff et al. 2019).

Due to the scarcity of cosmogenic nuclides (10^{-12} or less compared with the stable isotopes), quantifying their abundances requires highly sensitive analytical techniques, such as accelerator mass spectrometry (AMS). Advances in AMS since the late 1990s have allowed us to use these nuclides—especially Be—as prominent tracers in the ocean and Earth sciences (Brown et al. 1988, 1992a,b; Lal 1991; McHargue & Damon 1991; von Blanckenburg et al. 2012; Yokoyama et al. 2016, 2019b). This article presents recent developments in the field and how Be isotopes can be used in marine, terrestrial, coastal, and glacial environments to elucidate a wide range of processes.

2. ACCELERATOR MASS SPECTROMETRY

An AMS system is a mass spectrometer incorporating an accelerator that can detect long-lived radioactive isotopes—namely, nuclides that exist in extremely small amounts in nature—with ultrahigh sensitivity. Attempts had been made to detect these nuclides before the development of AMS, such as an analysis of ^{3}He using a cyclotron at the University of California, Berkeley (Alvarez & Cornog 1939), and a 1977 attempt at Lawrence Berkeley National Laboratory to analyze ^{14}C (Muller 1977), but once tandem electrostatic accelerators became available (Bennett et al. 1978), the field exploded. A tandem accelerator is a type of electrostatic accelerator where the beam entrance and exit are at ground potential, and the central terminal holds the highest voltage. It accumulates electric charge to generate voltage in the megavolt range (typically $<$10 MV). Negative ions are accelerated toward the terminal, which passes through a charge conversion device (stripper) where electrons are stripped, forming positive ions. When the charge is converted, the particles are accelerated again, and if the charge state is higher (more highly charged), the energy gain increases. This two-stage acceleration is the reason why these systems are called tandem accelerators.

In AMS-based Be analysis, the ^{10}Be/^{9}Be ratio is measured with a sensitivity ranging from 10^{-15} to 10^{-11}. This is achieved by counting the rare isotopes (^{10}Be) and measuring the current of the abundant isotopes (^{9}Be). The importance of AMS lies in the complete separation and counting of trace components, making the use of an accelerator essential. Negative ions must be injected into the system using a Cs sputter-type solid negative ion source for tandem AMS. Heated Cs vapor ionizes on the ionizer surface, forming Cs^{+}, which is accelerated toward the target, sputtering the target while forming a Cs layer on the surface, providing electrons to generate negative ions (Middleton 1989, Southon & Santos 2004). The generated negative ions are then accelerated, extracted, and injected into the analysis system. Atoms with high electron affinity are more likely to form negative ions. Conversely, elements with low electron affinity are not well-suited for this type of system. Thus, for $^{10}Be^{-}$ AMS, $^{10}BeO^{-}$ is used instead of ^{10}Be (Imamura et al. 1984). The ionization efficiency is typically below a few percent and depends on the condition of the ion source.

Separation of ^{10}B using magnetic or electrostatic fields is difficult since ^{10}B has the same mass as ^{10}Be and is a significant interference. Clear separation is needed because ions with the same mass or charge may enter the final detector. In AMS, ions accelerated to megaelectronvolt-level energies utilize radiation detection techniques to measure energy loss due to interactions with matter. Applying an electric field allows the collection of ionized electrons to measure ion energy, with semiconductor detectors and gas counters operating based on this principle. As ions pass through a medium, they decelerate due to interactions with electrons. If their velocity is high, they reach a full-strip state, where energy loss is proportional to Z^2 (the Bethe–Bloch formula) (Ziegler 1999). Thus, atoms with higher atomic numbers ionize more electrons at the initial stage.

As energy decreases, ionization and recombination occur repeatedly, but differences in average charge allow for separation. ^{10}Be and ^{10}B have different energy losses, with the larger atomic number of B causing greater energy loss, which allows for efficient removal of ^{10}B from ^{10}Be in the preliminary stage, improving measurement accuracy. However, due to energy straggling, some ^{10}B remains in a high-energy state, making thorough removal during preprocessing crucial. Recent improvements in chemical processing techniques have led to the establishment of low-B-contamination preprocessing methods (Yokoyama et al. 2019b), expanding the application of Be-based research in the field of marine sciences.

3. MARINE ENVIRONMENT

The different sources of ^{10}Be and ^{9}Be lead to distinct surface-water concentrations in the global oceans. In regions of high precipitation, such as the northwest Pacific, surface waters are enriched in ^{10}Be, leading to relatively high ^{10}Be/^{9}Be ratios of $\sim 2 \times 10^{-7}$ (Kusakabe et al. 1987, 1990; Ku et al. 1990) (**Figure 2*a***). In regions close to major rivers, such as the Eurasian Basin, which receives Siberian river water (**Figure 2*a***), or aeolian inputs, such as the equatorial Atlantic proximal to Saharan dust plumes, surface waters are enriched in ^{9}Be, leading to relatively low ^{10}Be/^{9}Be ratios of $\sim 0.3 \times 10^{-7}$ (Kusakabe et al. 1990, Luo & Ku 2004, Frank et al. 2009). Be sources can be distinguished using plots of relative Be concentration (e.g., von Blanckenburg et al. 2015), whereby gradients of <1 or >1 indicate that variations are controlled by dilution and scavenging efficiency but with additional contributions of ^{10}Be or ^{9}Be, respectively (**Figure 2*b***).

If surface inputs of ^{10}Be or ^{9}Be are generally absent, then the high scavenging potential of Be causes concentrations to follow a nutrient-like profile that leads to constant ^{10}Be/^{9}Be ratios with depth and a gradient close to 1, as observed in the equatorial Pacific (Kusakabe et al. 1987, 1990; Anderson et al. 1990; Lao et al. 1992; Wilson et al. 2013) (**Figure 2**). In deeper waters, the shorter residence time of Be (200–1,200 years) when compared with the mixing time of the ocean leads to an enrichment of ^{10}Be in the Pacific, associated with the nutrient effect, and ^{9}Be in the

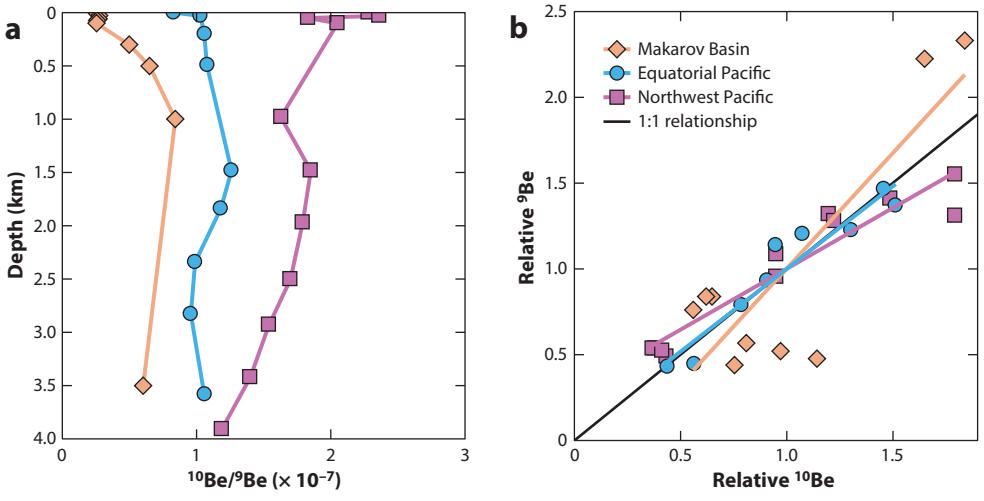

Figure 2

(*a*) Be isotope ratios and (*b*) relative ^{10}Be versus relative ^{9}Be relationships for depth profiles from the Makarov Basin (*orange diamonds*), equatorial Pacific (*blue circles*), and northwest Pacific (*purple squares*). The black line in panel *b* represents a 1:1 relationship. Data are from Kusakabe et al. (1987) and Frank et al. (2009).

Atlantic, due to higher terrestrial inputs (Anderson et al. 1990, Ku et al. 1990, Peng et al. 1990, Lao et al. 1992, von Blanckenburg et al. 1996). Therefore, the $^{10}Be/^{9}Be$ ratio of deep waters increases along the advective flow line: North Atlantic (~0.6) < South Atlantic (~0.7) < Circumpolar Deep Water (~0.9) < Pacific (~1.2) (Kusakabe et al. 1990). The behavior of Be in surface waters and at depth has allowed Be isotopes to become a quasi-conservative tracer of ocean circulation and water mass mixing that can overcome limitations associated with other geochemical proxies (von Blanckenburg et al. 1996; Frank et al. 2002, 2009; Wilson et al. 2013; Kong et al. 2021).

4. TERRESTRIAL ENVIRONMENT

On land, meteoric ^{10}Be is scavenged by particles in lakes and rivers, where it is deposited in underlying sediments or is readily absorbed to particles in the top few meters of soil profiles, subsequently decaying with a half-life of 1.39 My (Nishiizumi et al. 2007, Chmeleff et al. 2010, Korschinek et al. 2010, Willenbring & von Blanckenburg 2010b). In stable, noneroding soils, if the amount of ^{10}Be can be measured and the flux of meteoric ^{10}Be can be estimated, the age of the soil since exposure to precipitation can be calculated (Barg et al. 1997, Willenbring & von Blanckenburg 2010b). If the accumulation of ^{10}Be within the soil profile is at steady state with the loss from erosion, as in recently exposed glacial sediments, then the inventory of ^{10}Be can instead be used to calculate local erosion rates (Brown et al. 1988, Graly et al. 2010, Willenbring & von Blanckenburg 2010b). Measurements of particle-bound ^{10}Be in surface soils and river sediments provide further applications for determining local and catchment-wide erosion rates, respectively (Jungers et al. 2009, Willenbring & von Blanckenburg 2010b, Wittmann et al. 2015, Wittman & von Blanckenburg 2016). However, this method is applicable only if riverine sorting has not introduced a grain-size effect on sediment ^{10}Be concentrations and where ^{10}Be is fully retentive in the weathering zone, which does not occur under acidic conditions (You et al. 1989, Willenbring & von Blanckenburg 2010b).

Normalizing meteoric ^{10}Be with ^{9}Be can overcome these limitations if the ^{9}Be concentration in the parent rock (~2.5 ppm in silicates) is known, both isotopes have equilibrated between the weathering fluids and the reactive solids formed during rock decomposition, and the flux into and out of the weathering zone is at steady state (von Blanckenburg et al. 2012). The $^{10}Be/^{9}Be$ ratio of soils and rivers depends on the flux of meteoric ^{10}Be, the landscape's denudation rate, and the fraction of ^{9}Be released during weathering reactions (von Blanckenburg et al. 2012). On the basis of these relationships, the isotope ratios of Be dissolved in rivers or absorbed/coprecipitated (hereafter referred to as the reactive phase) into secondary solids can be used to calculate denudation rates or weathering intensity at the terrestrial or catchment scale (Lebatard et al. 2010; von Blanckenburg et al. 2012, 2015).

The $^{10}Be/^{9}Be$ of the reactive phase—consisting of adsorbed Be and Be coprecipitated into amorphous and crystalline phases, such as Mn-Fe oxyhydroxides chemically extracted from fluvial sediments and the riverine dissolved phase of the Amazon and Orinoco Basins—has been used to successfully reconstruct denudation and weathering rates that are in agreement with independent measurements, suggesting that chemical weathering in Amazon tributaries is relatively low (Brown et al. 1992a; Wittmann et al. 2012, 2015; Wittmann & von Blanckenburg 2016). A similar application of $^{10}Be/^{9}Be$ ratios in the reactive phase of suspended sediments from the Ganges Basin revealed a decrease in denudation rates from the Himalayas (0.5 mm y^{-1}) to the lowlands (0.17 mm y^{-1}), indicating a short sediment transfer time and lower degree of weathering in floodplain areas (Rahaman et al. 2017). Further application to Taiwanese rivers found a fourfold range in denudation rates due to stochastic landsliding and placed an upper global denudation rate of >30 mm y^{-1} (Deng et al. 2020, 2021), while other studies were able to quantify weathering and

erosion rates in the Potomac Basin and the northwest Czech Republic (Dannhaus et al. 2018, Portenga et al. 2019).

5. COASTAL ENVIRONMENT

During transport from river catchments to the open ocean, Be is removed or enriched in estuaries due to the high particle reactivity of Be at near-neutral pH (Measures & Edmond 1983, You et al. 1989, Brown et al. 1992b). The addition of Be in the Ganges, the Yangtze, the Pearl River, Zrmanja, and Loch Etive is likely caused by release from sediments or desorption from particulate matter (Edmond 1983, Measures & Edmond 1983, Kusakabe et al. 1991, Suhrhoff et al. 2019). Conversely, the amount of Be removal observed in the Amazon estuary and Congo River is dependent on the relative proportion of organic versus inorganic colloids (Measures & Edmond 1983, Brown et al. 1992a, Suhrhoff et al. 2019). Complexation with organic colloids (namely, humic and fulvic acids) can facilitate Be transport across estuaries, while the presence of inorganic colloids (such as Fe, Mn, and Al oxyhydroxides; clays; and other forms of silica) removes Be from solution (Measures & Edmond 1983, Suhrhoff et al. 2019). Furthermore, organic colloids speciated as Be-humate can complex with hydroxide coatings and clay minerals, amplifying the removal of Be by inorganic colloids (Takahashi et al. 1999, Willenbring & von Blanckenburg 2010b, Suhrhoff et al. 2019).

Due to Be removal in estuaries, only 13–30% of marine ^{9}Be is derived from the dissolved load of rivers (von Blanckenburg & Bouchez 2014, Suhrhoff et al. 2019, Deng et al. 2023). Additional ^{9}Be is sourced from early diagenetic release of particle-bound reactive Be at the sediment–water interface (von Blanckenburg & Bouchez 2014, Suhrhoff et al. 2019, Deng et al. 2023). On continental shelves, the abundant particle supply of mainly Mn-Fe oxides coupled to strong redox cycling in porewater leads to a benthic ^{9}Be flux that is approximately double the dissolved riverine flux (Deng et al. 2023). When combined with diagenetic release from slope and deep-sea sediments, the benthic flux represents the largest source of ^{9}Be to the oceans (62 $\pm$ 16%). The remaining marine input of ^{9}Be is sourced from the dissolution of silicate-bearing aeolian dust in the ocean (~12%) (von Blanckenburg & Bouchez 2014, Deng et al. 2023).

The order-of-magnitude-higher ^{10}Be concentration in seawater relative to river water leads to high ^{10}Be/^{9}Be variability in sediment phases from the coast to the shelf slope (Wittmann et al. 2017, Bernhardt et al. 2020). The reactive phase of shelf sediments represents coprecipitation of two authigenic rims: one incorporated from rivers with low terrestrial ^{10}Be/^{9}Be ratios ($\sim 2 \times 10^{-7}$) and an ocean-derived rim with high marine ^{10}Be/^{9}Be ratios ($\sim 1 \times 10^{-7}$) (Wittmann et al. 2017). In sites proximal to the coast, the reactive phase will likely record fluvial ratios, unaffected by seawater exchange, that can be used to study erosion rates, whereas sites farther offshore, below a well-mixed water column, will record a seawater signature representing the basin-scale weathering and denudation flux (Wittmann et al. 2017).

6. THE BERYLLIUM CONUNDRUM

The Cenozoic Era began approximately 65 Ma and has experienced continuous cooling since the end of the much warmer Mesozoic period, when ice sheets were absent. This cooling is explained by a decrease in atmospheric pCO_2 due to an increase in ocean alkalinity as a result of mountain building, including the collision of the Indian subcontinent with the Eurasian continent, the formation of the Andes and Alps, and increased global glacial activity (e.g., Raymo et al. 1988, Ruddiman & Kutzbach 1989, Herman et al. 2013, Wilner et al. 2024). Terrestrial weathering and erosion deliver detrital materials to the ocean, which are recorded in sediments. An increasing flux of silicate minerals into the ocean has been characterized by several geological and geochemical proxies. An increased sediment supply has been reported globally during this period

(Müller et al. 2022), which could trap organic matter to sequester carbon. Seawater chemistry records have shown an increase in terrigenous inputs recorded as strontium isotopes (Hodell et al. 1989, 2007), lithium isotopes (Misra & Froelich 2012), osmium isotopes (Peucker-Ehrenbrink & Ravizza 2000), and a deepening of the carbonate compensation depth (Campbell et al. 2018, Derry 2022).

However, the silicate weathering feedback—that is, changes in ocean chemistry caused by silicate weathering—is so effective that the temperature of the Earth's surface would have been brought below freezing within a million years or so if the source of CO_2 to the atmosphere were driven mainly by volcanic activity, similar to today, to prevent the climate from going into a runaway icehouse state (Berner & Caldeira 1997). Additional sources of CO_2 to the atmosphere are needed to close the mass balance of the global carbon cycle, and several candidates have been proposed, such as carbonate dissolution induced by pyrite oxidation (Torres et al. 2014, Hilton & West 2020), oxidation of organic carbon due to mountain glaciation (Horan et al. 2017), reduction of basalt weathering (Li & Elderfield 2013), and metamorphism (Bickle 1996).

Recent studies using Be isotopes show a different picture. The ratio of the two isotopes has been relatively constant during the last 12 My in the Pacific, Atlantic, and Arctic Oceans (Willenbring & von Blanckenburg 2010a). High-resolution measurements of Be for the last 2 My were also performed to look at the behavior of Be isotopes in the ocean during glacial and interglacial cycles, and no major changes were observed (von Blanckenburg et al. 2015). The contradiction between conventional views of Neogene cooling due to seawater chemistry changes derived from tectonic activities and the constant erosion scenario based on Be isotopes has been referred to as the Be conundrum (Li et al. 2021). A lead isotope study for the last 550,000 years showed that physical and chemical weathering could be in balance and that basin-scale influences are canceled out (Foster & Vance 2006). To satisfy the observations from Be signatures and other proxies, spatial variations of intensified weathering sites have been proposed, showing that the global climate system has plasticity to adjust its feedback system by changing the surface reactivity of weathering surfaces (Caves Rugenstein et al. 2019, von Blanckenburg et al. 2022).

The other proposals for reconciliations that focus on shelf removal rates use Be variations to explain constant isotope ratios through time (Li et al. 2021). Because of its strong particle affinity, Be entering via the rivers is trapped on the continental shelf, controlling the signals from the open oceans. The transport pathways from the river to the open ocean are still under debate and could potentially solve the puzzle (von Blanckenburg & Bouchez 2014, Suhrhoff et al. 2019). Dissolved Be isotopes entering the ocean are scavenged, and the affinity of Be is stronger for organic carbon and biogenic silica but not for carbonate (Chase et al. 2003, Chase & Anderson 2004, Kretschmer et al. 2011). Scavenged Be is also returned to the water column as particles degrade and sink to the seafloor (Bacon & Anderson 1982, Siddall et al. 2008, Deng et al. 2025). Therefore, the balance between the coastal trap of Be before mixing into the open ocean and the boundary exchange that releases reactive Be from land back into seawater is an important process (Bouchez et al. 2022, Deng et al. 2023) that will be a key focus for studies of the marine environment using Be isotopes.

7. GLACIAL ENVIRONMENT

Unlike temperate and tropical river catchments, Be isotopes in glacial systems are generally not well-mixed, leading to separate transport pathways for ^{10}Be and ^{9}Be across ice sheets and outlet glaciers (Graly et al. 2018). ^{10}Be produced in the atmosphere is delivered to a glacier via snow, becoming enriched throughout the ice column ($5–8 \times 10^4$ atoms g^{-1}), where it is stored until subsequent release through melting (Raisbeck & Yiou 1985, Beer et al. 1988, Raisbeck et al. 2007, Baroni et al. 2011). On the other hand, ^{9}Be is released during subglacial weathering and is

transported in basal sediments in the lower few meters of the deforming bed (Graly et al. 2018, White et al. 2019). Due to the unique behavior of Be in glacial environments, the reactive phase of marine and lake sediments can be used to reconstruct past changes in several glacial processes, such as subglacial erosion, meltwater flux, ice shelf circulation, and ice margin history, from the basin scale to individual ice streams.

7.1. Glacial Lakes, Marginal Seas, and Ocean Basins

The reactive phase of sediments from glacially fed lakes records the Be isotope variation of the dissolved and reactive load of local glacial catchments (Sproson et al. 2021). The major source of ^{10}Be to glacial lakes is surface and subglacial meltwater, with negligible inputs from marine and atmospheric sources (Behrens et al. 2019, Sproson et al. 2021). This ^{10}Be mixes with ^{9}Be released to the basal zone during erosion of the underlying bedrock (von Blanckenburg & Bouchez 2014, Sproson et al. 2021). Downcore ^{10}Be/^{9}Be variations in sediment cores from Lake Maruwan Oike and Lake Skallen along the Soya Coast of Lützow-Holm Bay (**Figure 3*a*,*b***), East Antarctica, were used to reconstruct meltwater and denudation flux changes during the Holocene [0–11.7 ka before present (BP)], revealing a substantial melting event at 4.2 ka BP coincident with a drier climate in North America, the Mediterranean, the Middle East, Africa, and South America and societal collapse of several civilizations (Nakamura et al. 2016, Yokoyama et al. 2019a, Sproson et al. 2021, Nemoto et al. 2024).

Baffin Bay, a subpolar oceanic basin, receives freshwater from Greenland, the Canadian Arctic, and the Atlantic Ocean. During glacial periods in the Earth's geological past, the Laurentide Ice Sheet (which covered most of modern-day North America), the Innuitian Ice Sheet, and the Greenland Ice Sheet formed a continuous ice belt surrounding Baffin Bay. Simon et al. (2016) measured ^{10}Be/^{9}Be and ^{230}Th excess in a sediment core from central Baffin Bay and observed a strong correlation with sedimentological parameters such as grain size and mineralogy driven by a shift from coarse, carbonate-rich inputs (lower ^{10}Be/^{9}Be) to fine-grained, feldspar-rich inputs (higher ^{10}Be/^{9}Be). Mass balance calculations suggested that denudation rates were relatively stable over the Last Glacial Period. However, six abrupt ice surging episodes, known as Heinrich events, resulted in a large input of glacially derived ^{10}Be, leading to a meltwater flux of ∼180 km^3 y^{-1}, consistent with ice sheet models (Simon et al. 2016).

Glacially derived ^{10}Be may also influence seawater concentrations at the ocean basin scale. Calving of icebergs transports approximately half the meltwater flux offshore past the continental shelf break (Rignot & Jacobs 2002), releasing ^{10}Be to surface waters (White et al. 2019). For example, meltwater derived from Antarctica has been attributed to an enrichment of ^{10}Be and high ^{10}Be/^{9}Be ratios (∼3.3 × 10^{-7}) in the Drake Passage (Kusakabe et al. 1987, Kusakabe et al. 1990). This mechanism largely avoids Be scavenging on the continental shelf, which removes up to 87% of Be (see Section 4), leading to a substantial flux of Be when compared with riverine inputs, but is likely insignificant when compared with ocean-wide flux from precipitation (von Blanckenburg & Bouchez 2014). However, the use of Be in marine sediments adjacent to major ice sheets has not been explored as a possible way to quantify past meltwater flux from iceberg calving.

7.2. Glaciated Margins

Understanding the complex interactions between the cryosphere and climate, ecosystems, and global sea level rise requires long-term records of ice mass loss that pre-date historical records (e.g., satellite observations since the 1960s). One way to obtain these records is through surface exposure dating of glacial deposits left behind following the retreat of a glacier since its local glacial maximum. Exposure dating relies on the fact that cosmogenic nuclides, such as ^{10}Be (e.g.,

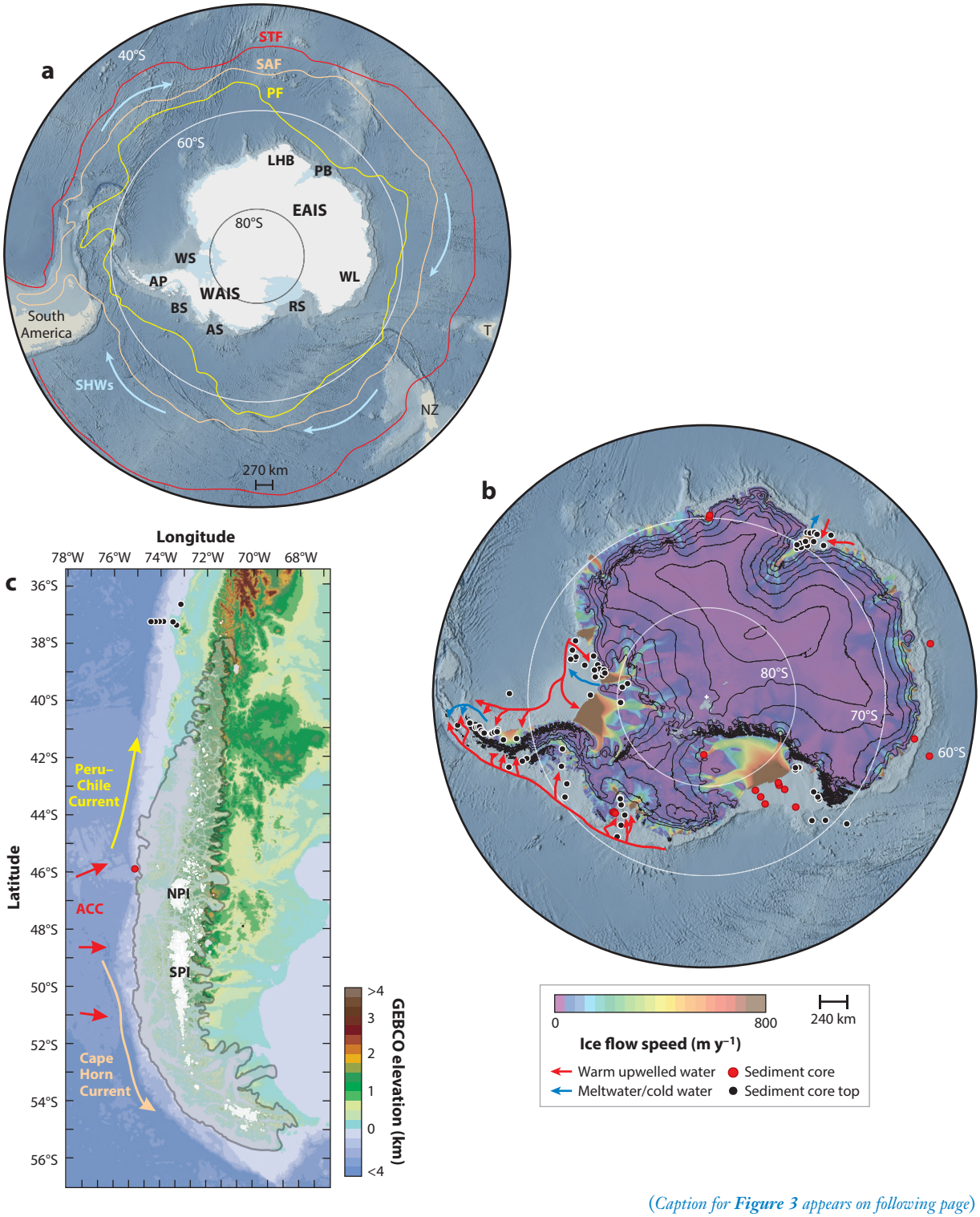

(*Caption for* ***Figure 3*** *appears on following page*)

Figure 3 (*Figure appears on preceding page*)

(*a*) Map of the Southern Hemisphere showing the Subtropical Front (STF), Subantarctic Front (SAF), and Polar Front (PF) of the Antarctic Circumpolar Current (ACC) and the direction of the Southern Hemisphere westerlies (SHWs). Also labeled are New Zealand (NZ), Tasmania (T), the West Antarctic Ice Sheet (WAIS), the East Antarctic Ice Sheet (EAIS), the Weddell Sea (WS), the Antarctic Peninsula (AP), the Bellingshausen Sea (BS), the Amundsen Sea (AS), the Ross Sea (RS), Wilkes Land (WL), Prydz Bay (PB), Lützow-Holm Bay (LHB), and South America. (*b*) Ice velocity for the Antarctic Ice Sheet (Rignot et al. 2011, Mouginot et al. 2012) with a generalized shelf circulation (using modified data from Jeromson et al. 2024). Red and black circles represent sampling sites for sediment cores (Scherer et al. 1998; Sjunneskog et al. 2007; Yokoyama et al. 2016; Valletta et al. 2018; Behrens et al. 2019; Sproson et al. 2021, 2022; Behrens et al. 2022; Huang et al. 2024) and core tops (White et al. 2019, Rhee et al. 2022, Jeromson et al. 2024), respectively. (*c*) Map of South America displaying the positions of the modern Northern and Southern Patagonian Ice Fields (NPI and SPI, respectively) in relation to the Patagonian Ice Sheet during the local last glacial maximum (*translucent gray area*) based on findings from the PATICE database (Davies et al. 2020). Major ocean currents such as the ACC are denoted by red, yellow, and orange arrows. Red and black circles represent sampling sites for sediment cores (Sproson et al. 2024) and core tops (Wittmann et al. 2017). Panels *a* and *b* were constructed using Quantarctica from the Norwegian Polar Institute (Matsuoka et al. 2018); the bathymetry data in panel *c* are from the General Bathymetric Chart of the Oceans 2020 (GEBCO_2020) Grid (GEBCO Bathymetric Compilation Group 2020).

Fink et al. 2006; Yamane et al. 2011, 2015; Johnson et al. 2020), accumulate in situ within the rock surface when the ice cover is thin or absent. The concentration of these nuclides in rocks taken from different altitudes can therefore be used to derive both the timing and pace of glacial retreat—also known as the dipstick approach (e.g., Johnson et al. 2014, Davies et al. 2020, Johnson et al. 2020). As surface exposure dating has been reviewed extensively elsewhere (e.g., Davies et al. 2020, Bierman et al. 2021), we focus here on a novel method for reconstructing past margins of marine-terminating ice shelves that takes advantage of the different reactive Be concentrations in glaciomarine sediments on the continental shelf (**Figures 2** and **4**).

7.2.1. The Antarctic Ice Sheet. Early work in the Ross Sea, Antarctica, and the Antarctic Peninsula (**Figure 3*a***) proposed that following ice shelf retreat, atmospherically derived cosmogenic ^{10}Be began to accumulate at the seafloor (Scherer et al. 1998, Sjunneskog et al. 2007, Yokoyama et al. 2016, Jeong et al. 2018). Downcore variations of reactive ^{10}Be, in combination

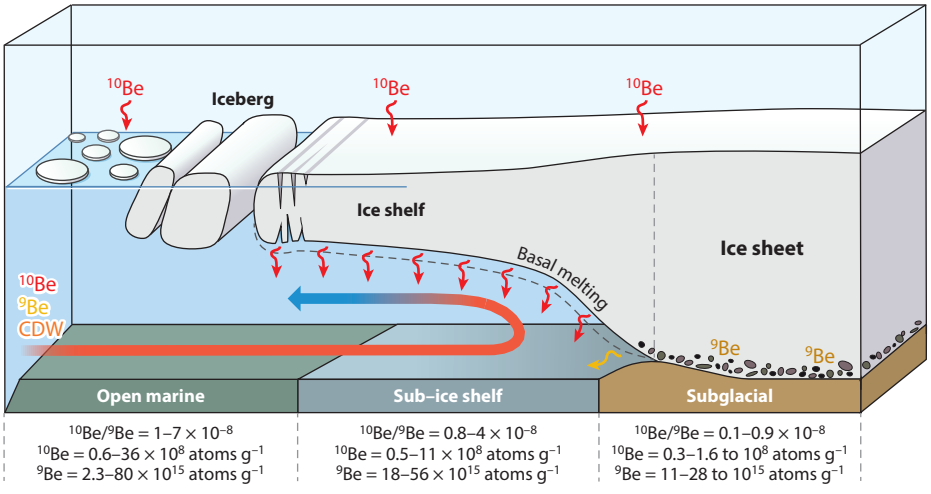

Figure 4

Processes influencing Be isotopes near a glaciated marine margin on the Antarctic continental shelf, based largely on Yokoyama et al. (2016), White et al. (2019), Sproson et al. (2022), and Jeromson et al. (2024). ^{10}Be can be supplied from atmospheric inputs, meltwater supply, and upwelling currents. Abbreviation: CDW, Circumpolar Deep Water.

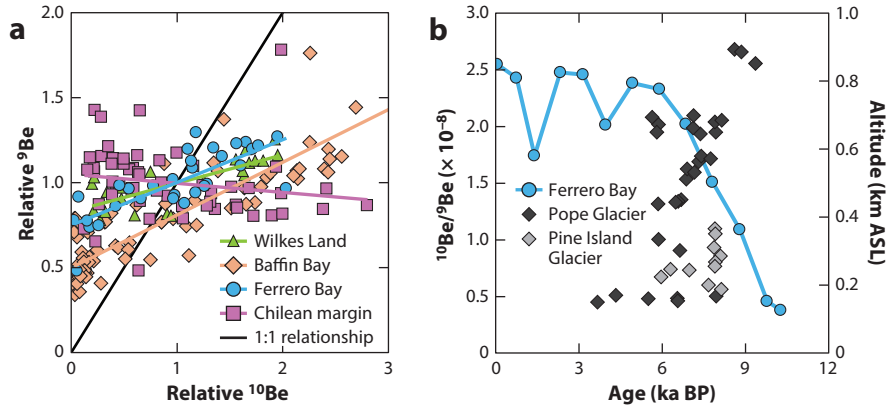

Figure 5

(*a*) Relative ^{10}Be versus relative ^{9}Be relationship for Wilkes Land (*green triangles*; Valletta et al. 2018), Baffin Bay (*orange diamonds*; Simon et al. 2016), Ferrero Bay (*blue circles*; Sproson et al. 2022), and the Chilean margin (*purple squares*; Sproson et al. 2024). The black line represents a 1:1 relationship. (*b*) ^{10}Be/^{9}Be ratios for Ferrero Bay (*blue circles*) compared with the thinning history of Pope Glacier (*black diamonds*) and Pine Island Glacier (*gray diamonds*), West Antarctica (Johnson et al. 2014, 2020; Sproson et al. 2022). Abbreviations: ASL, above sea level; BP, before present.

with compound-specific radiocarbon dating, were therefore able to constrain Ross Ice Shelf (**Figure 3*b***) breakup to ∼5 ka BP, reaching its current configuration by ∼1.5 ka BP, representing an ∼200–400-km retreat (Yokoyama et al. 2016). A thermodynamic ice shelf/ocean model indicates that this was the result of atmospheric warming combined with warm water upwelling onto the continental shelf (Yokoyama et al. 2016).

Subsequent Be isotope analysis of a sediment core from offshore Wilkes Land, East Antarctica (**Figure 3*a*,*b***), revealed large ^{10}Be/^{9}Be variation during the Pliocene (2.6–5.3 Ma), with maximum values during mild warming events just prior to the Mid-Pliocene Warm Period (Valletta et al. 2018). The relationship of relative ^{10}Be to relative ^{9}Be (see Section 3) from this site and other glaciated margins records a gradient less than 1 (**Figure 5*a***), suggesting an additional source of ^{10}Be to glaciomarine sediments that is driving the observed ^{10}Be/^{9}Be variation. Unlike previous work from the Ross Sea, mass balance calculations suggest that the fallout of ^{10}Be from the atmosphere is insufficient (<1% of measured ^{10}Be) to represent this additional source. Valletta et al. (2018) proposed that the release of ^{10}Be stored in Ninnis, Cook, and Mertz Glaciers through basal melting (**Figure 4**) was sufficient to drive the observed glacial–interglacial transitions, in a similar manner to subpolar basins and lakes (see Section 7.1).

A study of glaciomarine sediments from Ferrero Bay adjacent to the Amundsen Sea, West Antarctica (**Figure 3*a*,*b***), revealed an increase in ^{10}Be/^{9}Be ratios from subglacial to sub–ice shelf values between 9 and 6 ka BP, representing up to 40 km of grounding line retreat (Sproson et al. 2022) (**Figure 5**). This was related to retreat of the nearby Cosgrove Ice Shelf through a change in the depositional setting and greater input of glacially derived ^{10}Be (**Figure 4**) caused by poleward transition of the Southern Hemisphere westerlies (**Figure 3*a***) which brought warm, moist air from the tropical Pacific (Sproson et al. 2022). The reactive Be record from Ferrero Bay compares well to the thinning history of Pope and Pine Island Glaciers (**Figure 5*b***), suggesting an Amundsen Sea–wide melting event from the early to mid-Holocene (Johnson et al. 2014, 2020; Sproson et al. 2022). This highlights the further insight that can be gained by combining reactive Be records in glaciomarine sediments with exposure dating of terrestrial moraines.

New insights into the nature of reactive Be in glacial environments have been provided by the study of core tops from Antarctic coastal sediments (White et al. 2019, Rhee et al. 2022, Jeromson et al. 2024) (black circles in **Figure 3*b***). A general increasing trend in reactive ^{10}Be and ^{10}Be/^{9}Be ratios is observed from the subglacial to the sub–ice shelf to the open marine environment (White et al. 2019, Jeromson et al. 2024) (**Figure 4**). Further mass balance modeling suggests that only 2–36% of annual ^{10}Be delivery to the continental shelf is derived from meltwater. Instead, the majority of ^{10}Be (60–97%) is delivered by upwelling waters (e.g., Circumpolar Deep Water) onto the Antarctic continental shelf (Jeromson et al. 2024). Today, the flow path of warm upwelled waters (red arrows in **Figure 3*b***) represents a major source of Be to glaciomarine sediments in the Weddell Sea, the Bellingshausen Sea, the Amundsen Sea, and Prydz Bay and along the Antarctic Peninsula (White et al. 2019, Rhee et al. 2022, Jeromson et al. 2024). Downcore variations in Be isotopes have provided a record of Circumpolar Deep Water incursion, a major driver of ice shelf retreat, onto the continental shelf since the Last Glacial Period (Huang et al. 2024).

7.2.2. The Patagonian Ice Sheet. Outside of Antarctica, the Chilean continental shelf is the only previously glaciated marine margin that has been studied with respect to Be isotopes in the reactive phase (**Figure 3*c***). The modern Patagonian ice fields were once part of a larger Patagonian Ice Sheet (translucent gray area in **Figure 3*c***) that extended from 38°S to 55°S during the Last Glacial Period (Davies et al. 2020). A sediment core from a depth of ∼1.5 km offshore of the Northern Patagonian Ice Field (red circle in **Figure 3*c***) revealed large ^{10}Be/^{9}Be variability over the Last Glacial Period (0–90 ka BP) (**Figure 6**). Although sea level change, weatherability, and sedimentation rates may have played a role, downcore variations in the ^{10}Be/^{9}Be ratio were related to the relative proximity of the Patagonian Ice Sheet's marine-terminating margin (Sproson et al. 2024). During glacials, the Patagonian Ice Sheet was more expanded, bringing a low, freshwater-like ^{10}Be/^{9}Be source close to the depositional site. During interglacials, the Patagonian Ice Sheet was smaller, retreating ∼125 km closer to its modern configuration, and the reactive phase recorded higher, seawater-like ^{10}Be/^{9}Be ratios.

Sproson et al. (2024) were able to compare the variability in Southern Hemisphere midlatitude glaciers with Northern Hemisphere ice sheets and found that, although the timing of change was

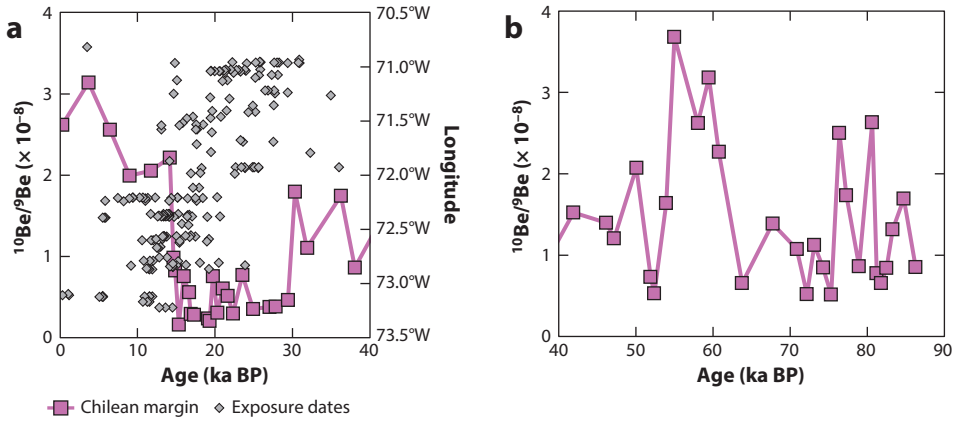

Figure 6

Be isotope record from the Chilean margin (*red circle* in **Figure 3*c***) over (*a*) 0–40 ka before present (BP) and (*b*) 40–90 ka BP (Sproson et al. 2024). The gray diamonds represent exposure dates east of the modern Northern Patagonian Ice Field (NPI) (73.2°W) from the PATICE database (Davies et al. 2020).

similar, discrepancies were caused by the effect of obliquity on the latitudinal position and strength of the Southern Hemisphere westerlies (**Figure 3*a***), which influenced the Antarctic Circumpolar Current (**Figure 3*c***) and the delivery of moisture to the Andes, which in turn feeds the Patagonian Ice Sheet (Sproson et al. 2024). The marine record compares well to exposure dating of glacial sediments from Patagonia, which shows a general retreat from an expanded easterly position to a near-modern configuration between 18 and 15 ka BP (Davies et al. 2020) (**Figure 6*a***). However, unlike the dipstick method, for which material prior to the last glacial episode is generally lacking, reactive Be isotopes in marine sediments can provide a continuous record of ice sheet margins over previous glacial cycles (**Figure 6*b***).

This study of the Patagonian Ice Sheet (Sproson et al. 2024) showed that downcore variations of reactive Be isotopes from glaciated margins follow a similar pattern to core tops across the Chilean continental shelf (black circles in **Figure 3*c***), as discussed in Section 5 (Wittmann et al. 2017). This suggests that Be isotopes are responding primarily to changes in the depositional setting, which is related to the relative proximity of the ice shelf or ice sheet (**Figure 4**). This, in turn, implies that although upwelling water masses onto the continental shelf may exert a major control on Antarctic glaciomarine sediments today (White et al. 2019, Jeromson et al. 2024), interpretations of downcore $^{10}Be/^{9}Be$ variation in relation to the presence of Circumpolar Deep Water should be treated with caution but will provide a powerful proxy for ice shelf history.

8. FUTURE ISSUES

The cosmogenic ^{10}Be produced in the atmosphere and its ratio to the stable ^{9}Be derived from terrestrial rocks through chemical weathering provide a powerful tracer for understanding Earth surface processes related to the carbon cycle. In particular, the ratio can be used to understand ice sheet behavior in the context of global sea level changes (Yokoyama & Purcell 2021).

An imbalance between global mean sea level and the sum of individual ice volumes during the Last Glacial Period creates an issue known as the missing ice problem, which has yet to be adequately solved (Nakada & Lambeck 1988; Yokoyama et al. 2018, 2022). Be isotopes can be applied to understand the melting history of Greenland and Antarctica through time using seafloor sediments, and when combined with other cosmogenic nuclides, such as compound-specific radiocarbon dating, to provide an accurate age model (e.g., Prothro et al. 2020), they could locate the missing ice.

Gaining a better understanding of ice sheet fluctuations from sediments will require more samples from ice fields and rivers. These datasets will be able to explain the $^{10}Be/^{9}Be$ in sediments from the continental shelf or slope and whether influences from ice melting or ocean mixing were dominant in the past. This could also be used to link variations in the strength of the Atlantic Meridional Overturning Circulation to global climate (e.g., Brendryen et al. 2020).

DISCLOSURE STATEMENT

The authors are not aware of any affiliations, memberships, funding, or financial holdings that might be perceived as affecting the objectivity of this review.

ACKNOWLEDGMENTS

This work was supported partly by the Japan Society for the Promotion of Science (JSPS) Grants-in-Aid for Scientific Research (KAKENHI) program (23KK0013, 23K20544, 24H00094, and 24K03074) and the Japan Science and Technology Agency (JST) Core Research for Evolutional Science and Technology (CREST) program (JPMJCR23J6).

LITERATURE CITED

Alvarez LW, Cornog R. 1939. Helium and hydrogen of mass 3. *Phys. Rev.* 56:613

Anderson R, Lao Y, Broecker WS, Trumbore SE, Hofmann HJ, Wolfli W. 1990. Boundary scavenging in the Pacific Ocean: a comparison of ^{10}Be and ^{231}Pa. *Earth Planet. Sci. Lett.* 96:287–304

Bacon MP, Anderson RF. 1982. Distribution of thorium isotopes between dissolved and particulate forms in the deep sea. *J. Geophys. Res. Oceans* 87:2045–56

Barg E, Lal D, Pavich M, Caffee M, Southon J. 1997. Beryllium geochemistry in soils: evaluation of ^{10}Be/^{9}Be ratios in authigenic minerals as a basis for age models. *Chem. Geol.* 140:237–58

Baroni M, Bard E, Petit JR, Magand O, Bourlés D. 2011. Volcanic and solar activity, and atmospheric circulation influences on cosmogenic ^{10}Be fallout at Vostok and Concordia (Antarctica) over the last 60 years. *Geochim. Cosmichim. Acta* 75:7132–45

Beer J, Siegenthaler U, Bonani G, Finkel RC, Oeschger H, et al. 1988. Information on past solar activity and geomagnetism from ^{10}Be in the Camp Century ice core. *Nature* 331:675–79

Behrens B, Miyairi Y, Sproson AD, Yamane M, Yokoyama Y. 2019. Meltwater discharge during the Holocene from the Wilkes subglacial basin revealed by beryllium isotope analysis of marine sediments. *J. Quat. Sci.* 34:603–8

Behrens BC, Yokoyama Y, Miyairi Y, Sproson AD, Yamane M, et al. 2022. Beryllium isotope variations recorded in the Adélie Basin, East Antarctica reflect Holocene changes in ice dynamics, productivity, and scavenging efficiency. *Quat. Sci. Adv.* 7:100054

Bennett C, Beukens R, Clover M, Elmore D, Gove H, et al. 1978. Radiocarbon dating with electrostatic accelerators: dating of milligram samples. *Science* 201:345–47

Berner RA, Caldeira K. 1997. The need for mass balance and feedback in the geochemical carbon cycle. *Geology* 25:955–56

Bernhardt A, Oelze M, Bouchez J, von Blanckenburg F, Mohtadi M, et al. 2020. ^{10}Be/^{9}Be ratios reveal marine authigenic clay formation. *Geophys. Res. Lett.* 47:e2019GL086061

Bickle M. 1996. Metamorphic decarbonation, silicate weathering and the long-term carbon cycle. *Terra Nova* 8:270–76

Bierman PR, Bender AM, Christ AJ, Corbett LB, Halsted CT, et al. 2021. Dating by cosmogenic nuclides. In *Encyclopedia of Geology*, ed. D Alderton, SA Elias. Academic Press. 2nd ed.

Bouchez J, von Blanckenburg F, Willenbring JK, Ibarra DE, Caves Rugenstein JK. 2022. There is no Neogene denudation conundrum. *PNAS* 119:e2202387119

Brendryen J, Haflidason H, Yokoyama Y, Haaga KA, Hannisdal B. 2020. Eurasian Ice Sheet collapse was a major source of Meltwater Pulse 1A 14,600 years ago. *Nat. Geosci.* 13:363–68

Brown ET, Edmond JM, Raisbeck GM, Bourlès DL, Yiou F, Measures CI. 1992a. Beryllium isotope geochemistry in tropical river basins. *Geochim. Cosmochim. Acta* 56:1607–24

Brown ET, Measures CI, Edmond JM, Bourlès DL, RG M, Yiou F. 1992b. Continental inputs of beryllium to the oceans. *Earth Planet. Sci. Lett.* 114:101–11

Brown L, Pavich MJ, Hickman R, Klein J, Middleton R. 1988. Erosion of the eastern United States observed with ^{10}Be. *Earth Surf. Process. Landf.* 13:441–57

Campbell SM, Moucha R, Derry LA, Raymo ME. 2018. Effects of dynamic topography on the Cenozoic carbonate compensation depth. *Geochem. Geophys. Geosyst.* 19:1025–34

Carcaillet J, Bourlès DL, Thouveny N, Arnold M. 2004. A high resolution authigenic ^{10}Be/^{9}Be record of geomagnetic moment variations over the last 300 ka from sedimentary cores of the Portuguese margin. *Earth Planet. Sci. Lett.* 219:397–412

Carcaillet JT, Thouveny N, Bourlés DL. 2003. Geomagnetic moment instability between 0.6 and 1.3 Ma from cosmonuclide evidence. *Geophys. Res. Lett.* 30:1792

Caves Rugenstein JK, Ibarra DE, von Blanckenburg F. 2019. Neogene cooling driven by land surface reactivity rather than increased weathering fluxes. *Nature* 571:99–102

Chase Z, Anderson RF. 2004. Comment on "On the importance of opal, carbonate, and lithogenic clays in scavenging and fractionating ^{230}Th, ^{231}Pa and ^{10}Be in the ocean" by S. Luo and T.-L. Ku. *Earth Planet. Sci. Lett.* 220:213–22

Chase Z, Anderson RF, Fleisher MQ, Kubik PW. 2003. Scavenging of ^{230}Th, ^{231}Pa and ^{10}Be in the Southern Ocean (SW Pacific sector): the importance of particle flux, particle composition and advection. *Deep-Sea Res. II* 50:739–68

Chmeleff J, von Blanckenburg F, Kossert K, Jakob D. 2010. Determination of the ^{10}Be half-life by multicollector ICP-MS and liquid scintillation counting. *Nucl. Instrum. Methods Phys. Res. B* 268:192–99

Dannhaus N, Wittmann H, Krám P, Christl M, von Blanckenburg F. 2018. Catchment-wide weathering and erosion rates of mafic, ultramafic, and granitic rock from cosmogenic meteoric ^{10}Be/^{9}Be ratios. *Geochim. Cosmochim. Acta* 222:618–41

Davies BJ, Darvill CM, Lovell H, Bendle JM, Dowdeswell JA, et al. 2020. The evolution of the Patagonian Ice Sheet from 35 ka to the present day (PATICE). *Earth-Sci. Rev.* 204:103152

Deng K, de Souza GF, Du J. 2025. Modern oceanic cycle of beryllium isotopes assessed using a data-constrained biogeochemical model. *Geochim. Cosmochim. Acta* 389:186–99

Deng K, Rickli J, Suhrhoff TJ, Du J, Scholz F, et al. 2023. Dominance of benthic fluxes in the oceanic beryllium budget and implications for paleo-denudation records. *Sci. Adv.* 9:eadg3702

Deng K, Wittmann H, Yang S, von Blanckenburg F. 2021. The upper limit of denudation rate measurement from cosmogenic ^{10}Be (meteoric)/^{9}Be ratios in Taiwan. *J. Geophys. Res. Earth Surf.* 126:e2021JF006221

Deng K, Yang S, von Blanckenburg F, Wittmann H. 2020. Denudation rate changes along a fast-eroding mountainous river with slate headwaters in Taiwan from ^{10}Be (meteoric)/^{9}Be ratios. *J. Geophys. Res. Earth Surf.* 125:e2019JF005251

Derry LA. 2022. Carbonate weathering, CO_2 redistribution, and Neogene CCD and pCO_2 evolution. *Earth Planet. Sci. Lett.* 597:117801

Edmond JM. 1983. The geochemical cycle of ^{9}Be: a reconnaissance. *Earth Planet. Sci. Lett.* 66:101–10

Field CV, Schmidt GA, Koch D, Salyk C. 2006. Modeling production and climate-related impacts on ^{10}Be concentration in ice cores. *J. Geophys. Res. Atmos.* 111:D15107

Fink D, McKelvey B, Hambrey MJ, Fabel D, Brown R. 2006. Pleistocene deglaciation chronology of the Amery Oasis and Radok Lake, northern Prince Charles Mountains, Antarctica. *Earth Planet. Sci. Lett.* 243:229–43

Foster GL, Rohling EJ. 2013. Relationship between sea level and climate forcing by CO_2 on geological timescales. *PNAS* 110:1209–14

Foster GL, Royer DL, Lunt DJ. 2017. Future climate forcing potentially without precedent in the last 420 million years. *Nat. Commun.* 8:14845

Foster GL, Vance D. 2006. Negligible glacial–interglacial variation in continental chemical weathering rates. *Nature* 444:918–21

Frank M, Porcelli D, Andersson P, Baskaran M, Björk G, et al. 2009. The dissolved beryllium isotope composition of the Arctic Ocean. *Geochim. Cosmochim. Acta* 73:6114–33

Frank M, van der Loeff MR, Kubik PW, Mangini A. 2002. Quasi-conservative behaviour of ^{10}Be in deep waters of the Weddell Sea and the Atlantic sector of the Antarctic Circumpolar Current. *Earth Planet. Sci. Lett.* 201:171–86

GEBCO Bathymetric Compilation Group. 2020. *The GEBCO_2020 Grid—a continuous terrain model of the global oceans and land*. Published Data Library, British Oceanographic Data Centre, National Oceanography Centre, Natural Environment Research Council. **https://doi.org/10.5285/a29c5465-b138-234d-e053-6c86abc040b9**

Graly JA, Bierman PR, Reusser LJ, Pavich MJ. 2010. Meteoric ^{10}Be in soil profiles—a global meta-analysis. *Geochim. Cosmochim. Acta* 74:6814–29

Graly JA, Corbett LB, Bierman PR, Lini A, Neumann TA. 2018. Meteoric ^{10}Be as a tracer of subglacial processes and interglacial surface exposure in Greenland. *Quat. Sci. Rev.* 191:118–31

Heikkilä U, Beer J, Abreu JA, Steinhilber F. 2013. On the atmospheric transport and deposition of the cosmogenic radionuclides (^{10}Be): a review. *Space Sci. Rev.* 176:321–32

Heikkilä U, Beer J, Feichter J. 2009. Meridional transport and deposition of atmospheric ^{10}Be. *Atmos. Chem. Phys.* 9:515–27

Henken-Mellies WU, Beer J, Heller F, Hsü KJ, Shen C, et al. 1990. ^{10}Be and ^{9}Be in South Atlantic DSDP Site 519: relation to geomagnetic reversals and to sediment composition. *Earth Planet. Sci. Lett.* 98:267–76

Herman F, Seward D, Valla PG, Carter A, Kohn B, et al. 2013. Worldwide acceleration of mountain erosion under a cooling climate. *Nature* 504:423–26

Hilton RG, West AJ. 2020. Mountains, erosion and the carbon cycle. *Nat. Rev. Earth Environ.* 1:284–99

Hodell DA, Kamenov GD, Hathorne EC, Zachos JC, Röhl U, Westerhold T. 2007. Variations in the strontium isotope composition of seawater during the Paleocene and early Eocene from ODP Leg 208 (Walvis Ridge). *Geochem. Geophys. Geosyst.* 8:Q09001

Hodell DA, Mueller PA, McKenzie JA, Mead GA. 1989. Strontium isotope stratigraphy and geochemistry of the late Neogene ocean. *Earth Planet. Sci. Lett.* 92:165–78

Horan K, Hilton RG, Selby D, Ottley CJ, Gröcke DR, et al. 2017. Mountain glaciation drives rapid oxidation of rock-bound organic carbon. *Sci. Adv.* 3:e1701107

Huang Z, Yokoyama Y, Behrens BC, Miyairi Y, Aze T, et al. 2024. Melting of Totten Glacier, East Antarctica since the Last Glacial Maximum revealed by beryllium isotope ratios of marine sediment. *Glob. Planet. Change* 241:104548

Imamura M, Hashimoto Y, Yoshida K, Yamane I, Yamashita H, et al. 1984. Tandem accelerator mass spectrometry of $^{10}Be/^{9}Be$ with internal beam monitor method. *Nucl. Instrum. Methods Phys. B* 5:211–16

Jagoutz O, Macdonald FA, Royden L. 2016. Low-latitude arc–continent collision as a driver for global cooling. *PNAS* 113:4935–40

Jeong A, Lee JI, Seong YB, Balco G, Yoo K-C, et al. 2018. Late Quaternary deglacial history across the Larsen B embayment, Antarctica. *Quat. Sci. Rev.* 189:134–48

Jeromson MR, Fujioka T, Fink D, Simon K, Smith J, et al. 2024. Circumpolar Deep Water upwelling is a primary source of ^{10}Be in Antarctic continental shelf sediments. *Glob. Planet. Change* 236:104424

Johnson JS, Bentley MJ, Smith JA, Finkel RC, Rood DH, et al. 2014. Rapid thinning of Pine Island Glacier in the early Holocene. *Science* 343:999–1001

Johnson JS, Roberts SJ, Rood DH, Pollard D, Schaefer JM, et al. 2020. Deglaciation of Pope Glacier implies widespread early Holocene ice sheet thinning in the Amundsen Sea sector of Antarctica. *Earth Planet. Sci. Lett.* 548:116501

Jungers MC, Bierman PR, Matmon A, Nichols K, Larsen J, Finkel R. 2009. Tracing hillslope sediment production and transport with in situ and meteoric ^{10}Be. *J. Geophys. Res. Earth Surf.* 114:F04020

Knudsen MF, Henderson GM, Frank M, Mac Niocaill C, Kubik PW. 2008. In-phase anomalies in Beryllium-10 production and palaeomagnetic field behaviour during the Iceland Basin geomagnetic excursion. *Earth Planet. Sci. Lett.* 265:588–99

Kong WY, Zhou LP, AsterTeam. 2021. Tracing water masses and assessing boundary scavenging intensity with beryllium isotopes in the northern South China Sea. *J. Geophys. Res. Oceans* 126:e2021JC017236

Korschinek G, Bergmaier A, Faestermann T, Gerstmann U, Knie K, et al. 2010. A new value for the half-life of ^{10}Be by heavy-ion elastic recoil detection and liquid scintillation counting. *Nucl. Instrum. Methods Phys. Res. B* 268:187–191

Kretschmer S, Geibert W, van der Loeff MMR, Schnabel C, Xu S, Mollenhauer G. 2011. Fractionation of ^{230}Th, ^{231}Pa, and ^{10}Be induced by particle size and composition within an opal-rich sediment of the Atlantic Southern Ocean. *Geochim. Cosmochim. Acta* 75:6971–87

Ku T, Kusakabe M, Measures C, Southon J, Cusimano G, et al. 1990. Beryllium isotope distribution in the western North Atlantic: a comparison to the Pacific. *Deep-Sea Res. A* 37:795–808

Kusakabe M, Ku TL, Southon JR. 1990. Beryllium isotopes in the ocean. *Geochem. J.* 24:263–72

Kusakabe M, Ku TL, Southon JR, Liu S, Vogel JS, et al. 1991. Be isotopes in rivers/estuaries and their oceanic budgets. *Earth Planet. Sci. Lett.* 102:265–76

Kusakabe M, Ku TL, Southon JR, Vogel JS, Nelson DE, et al. 1987. Distribution of ^{10}Be and ^{9}Be in the Pacific Ocean. *Earth Planet. Sci. Lett.* 82:231–40

Lal D. 1991. Cosmic ray labeling of erosion surfaces: in situ nuclide production rates and erosion models. *Earth Planet. Sci. Lett.* 104:424–39

Lal D, Peters B. 1967. Cosmic ray produced radioactivity on the Earth. In *Kosmische Strahlung II/Cosmic Rays II*, ed. K Sitte. Springer

Lao Y, Anderson RF, Broecker WS, Trumbore SE, Hofmann HJ, Wolfli W. 1992. Transport and burial rates of ^{10}Be and ^{231}Pa in the Pacific Ocean during the Holocene period. *Earth Planet. Sci. Lett.* 113:173–89

Larsen T, Yokoyama Y, Fernandes R. 2018. Radiocarbon in ecology: insights and perspectives from aquatic and terrestrial studies. *Methods Ecol. Evol.* 9:181–90

Lebatard AE, Bourlès DL, Braucher R, Arnold M, Duringer P, et al. 2010. Application of the authigenic $^{10}Be/^{9}Be$ dating method to continental sediments: reconstruction of the Mio-Pleistocene sedimentary sequence in the early hominid fossiliferous areas of the northern Chad Basin. *Earth Planet. Sci. Lett.* 297:57–70

Lee C-TA, Shen B, Slotnick BS, Liao K, Dickens GR, et al. 2013. Continental arc–island arc fluctuations, growth of crustal carbonates, and long-term climate change. *Geosphere* 9:21–36

Li G, Elderfield H. 2013. Evolution of carbon cycle over the past 100 million years. *Geochim. Cosmochim. Acta* 103:11–25

Li S, Goldstein SL, Raymo ME. 2021. Neogene continental denudation and the beryllium conundrum. *PNAS* 118:e2026456118

Luo S, Ku T-L. 2004. On the importance of opal, carbonate, and lithogenic clays in scavenging and fractionating ^{230}Th, ^{231}Pa and ^{10}Be in the ocean. *Earth Planet. Sci. Lett.* 220:201–11

Matsuoka K, Skoglund A, Roth G. 2018. *Quantarctica*. Dataset, Norwegian Polar Institute. **https://doi.org/10.21334/npolar.2018.8516e961**

McHargue L, Damon P. 1991. The global beryllium 10 cycle. *Rev. Geophys.* 29:141–58

Measures C, Edmond J. 1983. The geochemical cycle of ^{9}Be: a reconnaissance. *Earth Planet. Sci. Lett.* 66:101–10

Ménabréaz L, Thouveny N, Bourlès D, Deschamps P, Hamelin B, Demory F. 2011. The Laschamp geomagnetic dipole low expressed as a cosmogenic ^{10}Be atmospheric overproduction at ∼41 ka. *Earth Planet. Sci. Lett.* 312:305–17

Middleton R. 1989. *A Negative-Ion Cookbook*. Department of Physics, University of Pennsylvania

Misra S, Froelich PN. 2012. Lithium isotope history of Cenozoic seawater: changes in silicate weathering and reverse weathering. *Science* 335:818–23

Mouginot J, Scheuchl B, Rignot E. 2012. Mapping of ice motion in Antarctica using synthetic-aperture radar data. *Remote Sens.* 4:2753–67

Muller RA. 1977. Radioisotope dating with a cyclotron: the sensitivity of radioisotope dating is improved by counting atoms rather than decays. *Science* 196:489–94

Müller RD, Mather B, Dutkiewicz A, Keller T, Merdith A, et al. 2022. Evolution of Earth's tectonic carbon conveyor belt. *Nature* 605:629–39

Nakada M, Lambeck K. 1988. The melting history of the late Pleistocene Antarctic ice sheet. *Nature* 333:36–40

Nakamura A, Yokoyama Y, Maemoku H, Yagi H, Okamura M, et al. 2016. Weak monsoon event at 4.2 ka recorded in sediment from Lake Rara, Himalayas. *Quat. Int.* 397:349–59

Nemoto K, Yokoyama Y, Obrochta SP, Miyairi Y, Fujiwara O, et al. 2024. A lake at the Mt. Fuji (Lake Motosu) recording prolonged negative Arctic Oscillation as reduction of aeolian dust due to westerly pathways during the Holocene. *Paleoceanogr. Paleoclimatol.* 39:e2023PA004805

Nishiizumi K, Imamura M, Caffee MW, Southon JR, Finkel RC, McAninch J. 2007. Absolute calibration of ^{10}Be AMS standards. *Nucl. Instrum. Methods Phys. Res. B* 258:403–13

Peng TH, Ku TL, Southon J, Broecker WS. 1990. Factors controlling the distribution of ^{10}Be and ^{9}Be in the ocean. In *Mantle to Meteorites: A Garland of Perspectives*, ed. K Gopalan, VK Gaur, BLK Somayajulu, JD MacDougall. Indian Academy of Sciences

Peucker-Ehrenbrink B, Ravizza G. 2000. The marine osmium isotope record. *Terra Nova* 12:205–19

Portenga EW, Bierman PR, Trodick CD Jr. Greene SE, DeJong BD, et al. 2019. Erosion rates and sediment flux within the Potomac River basin quantified over millennial timescales using beryllium isotopes. *GSA Bull.* 131:1295–311

Prothro LO, Majewski W, Yokoyama Y, Simkins LM, Anderson JB, et al. 2020. Timing and pathways of East Antarctic ice sheet retreat. *Quat. Sci. Rev.* 230:106166

Rahaman W, Wittmann H, von Blanckenburg F. 2017. Denudation rates and the degree of chemical weathering in the Ganga River basin from ratios of meteoric cosmogenic ^{10}Be to stable ^{9}Be. *Earth Planet. Sci. Lett.* 469:156–69

Raisbeck GM, Yiou F. 1985. ^{10}Be in polar ice and atmospheres. *Ann. Glaciol.* 7:138–40

Raisbeck GM, Yiou F, Jouzel J, Stocker TF. 2007. Direct north-south synchronization of abrupt climate change record in ice cores using Beryllium 10. *Clim. Past* 3:541–47

Raymo ME, Ruddiman WF, Froelich PN. 1988. Influence of late Cenozoic mountain building on ocean geochemical cycles. *Geology* 16:649–53

Rhee HH, Seong YB, Lee MK, Jeong A, Dash C, et al. 2022. Spatial variations of authigenic beryllium isotopes in surface sediments of the Antarctic oceans: a proxy for sea ice dynamics and sedimentary environments. *Geosci. J.* 26:455–67

Rignot E, Jacobs SS. 2002. Rapid bottom melting widespread near Antarctic ice sheet grounding lines. *Science* 296:2020–23

Rignot E, Mouginot J, Scheuchl B. 2011. Ice flow of the Antarctic ice sheet. *Science* 333:1427–30

Robinson C, Raisbeck GM, Yiou F, Lehman B, Laj C. 1995. The relationship between ^{10}Be and geomagnetic field strength records in central North Atlantic sediments during the last 80 ka. *Earth Planet. Sci. Lett.* 136:551–57

Ruddiman WF, Kutzbach JE. 1989. Forcing of late Cenozoic northern hemisphere climate by plateau uplift in southern Asia and the American West. *J. Geophys. Res. Atmos.* 94:18409–27

Sakuramoto Y, Yamazaki T, Kimoto K, Miyairi Y, Kuroda J, et al. 2017. A geomagnetic paleointensity record of 0.6 to 3.2 Ma from sediments in the western equatorial Pacific and remanent magnetization lock-in depth. *J. Geophys. Res. Solid Earth* 122:7525–43

Scherer RP, Aldahan A, Tulaczyk S, Possnert G, Engelhardt H, Kamb B. 1998. Pleistocene collapse of the West Antarctic ice sheet. *Science* 281:82–85

Siddall M, Khatiwala S, van de Flierdt T, Jones K, Goldstein SL, et al. 2008. Towards explaining the Nd paradox using reversible scavenging in an ocean general circulation model. *Earth Planet. Sci. Lett.* 274:448–61

Simon Q, Bourlès DL, Bassinot F, Nomade S, Marino M, et al. 2017. Authigenic ^{10}Be/^{9}Be ratio signature of the Matuyama–Brunhes boundary in the Montalbano Jonico marine succession. *Earth Planet. Sci. Lett.* 460:255–67

Simon Q, Thouveny N, Bourlès DL, Nuttin L, Hillaire-Marcel C, St-Onge G. 2016. Authigenic ^{10}Be/^{9}Be ratios and ^{10}Be-fluxes ($^{230}Th_{xs}$-normalized) in central Baffin Bay sediments during the last glacial cycle: paleoenvironmental implications. *Quat. Sci. Res.* 140:142–62

Simon Q, Thouveny N, Bourlès DL, Valet J-P, Bassinot F. 2020. Cosmogenic ^{10}Be production records reveal dynamics of geomagnetic dipole moment (GDM) over the Laschamp excursion (20–60 ka). *Earth Planet. Sci. Lett.* 550:116547

Sjunneskog C, Scherer R, Aldahan A, Possnert G. 2007. ^{10}Be in glacial marine sediment of the Ross Sea, Antarctica, a potential tracer of depositional environment and sediment chronology. *Nucl. Instrum. Methods Phys. Res. B* 259:576–83

Southon JR, Santos GM. 2004. Ion source development at KCCAMS, University of California, Irvine. *Radiocarbon* 46:33–39

Sproson AD, Takano Y, Miyairi Y, Aze T, Matsuzaki H, et al. 2021. Beryllium isotopes in sediments from Lake Maruwan Oike and Lake Skallen, east Antarctica, reveal substantial glacial discharge during the late Holocene. *Quat. Sci. Rev.* 256:106841

Sproson AD, Yokoyama Y, Miyairi Y, Aze T, Clementi VJ, et al. 2024. Near-synchronous Northern Hemisphere and Patagonian Ice Sheet variation over the last glacial cycle. *Nat. Geosci.* 17:450–57

Sproson AD, Yokoyama Y, Miyairi Y, Aze T, Totten RL. 2022. Holocene melting of the West Antarctic Ice Sheet driven by tropical Pacific warming. *Nat. Commun.* 13:2434

Suhrhoff TJ, Rickli J, Crocket K, Bura-Nakic E, Vance D. 2019. Behavior of beryllium in the weathering environment and its delivery to the ocean. *Geochim. Cosmochim. Acta* 265:48–68

Takahashi Y, Minai Y, Ambe S, Makide Y, Ambe F. 1999. Comparison of adsorption behavior of multiple inorganic ions on kaolinite and silica in the presence of humic acid using the multitracer technique. *Geochim. Cosmochim. Acta* 63:815–36

Torres MA, West AJ, Li G. 2014. Sulphide oxidation and carbonate dissolution as a source of CO_2 over geological timescales. *Nature* 507:346–49

Valletta RD, Willenbring JK, Passchier S, Elmi C. 2018. ^{10}Be/^{9}Be ratios reflect Antarctic Ice Sheet freshwater discharge during Pliocene warming. *Paleoceanogr. Paleoclimatol.* 33:934–44

von Blanckenburg F, Bouchez J. 2014. River fluxes to the sea from the oceans $^{10}Be/^{9}Be$ ratio. *Earth Planet. Sci. Lett.* 387:34–43
von Blanckenburg F, Bouchez J, Ibarra DE, Maher K. 2015. Stable runoff and weathering fluxes into the oceans over Quaternary climate cycles. *Nat. Geosci.* 8:538–42
von Blanckenburg F, Bouchez J, Willenbring JK, Ibarra DE, Caves Rugenstein JK. 2022. There is no Neogene denudation conundrum. *PNAS* 119:e2202387119
von Blanckenburg F, Bouchez J, Wittmann H. 2012. Earth surface erosion and weathering from the ^{10}Be (meteoric)/^{9}Be ratio. *Earth Planet. Sci. Lett.* 351:295–305
von Blanckenburg F, O'Nions R, Belshaw N, Gibb A, Hein J. 1996. Global distribution of beryllium isotopes in deep ocean water as derived from FeMn crusts. *Earth Planet. Sci. Lett.* 141:213–26
White DA, Fink D, Post AL, Simon K, Galton-Fenzi B, et al. 2019. Beryllium isotope signatures of ice shelves and sub-ice shelf circulation. *Earth Planet. Sci. Lett.* 505:86–95
Willenbring JK, von Blanckenburg F. 2010a. Long-term stability of global erosion rates and weathering during late-Cenozoic cooling. *Nature* 465:211–14
Willenbring JK, von Blanckenburg F. 2010b. Meteoric cosmogenic Beryllium-10 adsorbed to river sediment and soil: applications for Earth-surface dynamics. *Earth-Sci. Rev.* 98:105–22
Wilner JA, Nordin BJ, Getraer A, Gregoire RM, Krishna M, et al. 2024. Limits to timescale dependence in erosion rates: quantifying glacial and fluvial erosion across timescales. *Sci. Adv.* 10:eadr2009
Wilson DJ, Piotrowski AM, Galy A, Clegg JA. 2013. Reactivity of neodymium carriers in deep sea sediments: implications for boundary exchange and paleoceanography. *Geochim. Cosmochim. Acta* 109:197–221
Wittmann H, von Blanckenburg F. 2016. The geological significance of cosmogenic nuclides in large lowland river basins. *Earth-Sci. Rev.* 159:118–41
Wittmann H, von Blanckenburg F, Bouchez J, Dannhaus N, Naumann R, et al. 2012. The dependence of meteoric ^{10}Be concentrations on particle size in Amazon River bed sediment and the extraction of reactive $^{10}Be/^{9}Be$ ratios. *Chem. Geol.* 318:126–38
Wittmann H, von Blanckenburg F, Dannhaus N, Bouchez J, Gaillardet J, et al. 2015. A test of the cosmogenic ^{10}Be (meteoric)/^{9}Be proxy for simultaneously determining basin-wide erosion rates, denudation rates, and the degree of weathering in the Amazon basin. *J. Geophys. Res. Earth Surf.* 120:2498–528
Wittmann H, von Blanckenburg F, Mohtadi M, Christl M, Bernhardt A. 2017. The competition between coastal trace metal fluxes and oceanic mixing from the $^{10}Be/^{9}Be$ ratio: implications for sedimentary records. *Geophys. Res. Lett.* 44:8443–276
Yamane M, Yokoyama Y, Abe-Ouchi A, Obrochta S, Saito F, et al. 2015. Exposure age and ice-sheet model constraints on Pliocene East Antarctic ice sheet dynamics. *Nat. Commun.* 6:7016
Yamane M, Yokoyama Y, Miura H, Maemoku H, Iwasaki S, Matsuzaki H. 2011. The last deglacial history of Lützow-Holm Bay, East Antarctica. *J. Quat. Sci.* 26:3–6
Yokoyama Y, Anderson JB, Yamane M, Simkins LM, Miyairi Y, et al. 2016. Widespread collapse of the Ross Ice Shelf during the late Holocene. *PNAS* 113:2354–59
Yokoyama Y, Esat TM, Thompson WG, Thomas AL, Webster JM, et al. 2018. Rapid glaciation and a two-step sea level plunge into the Last Glacial Maximum. *Nature* 559:603–7
Yokoyama Y, Hirabayashi S, Goto K, Okuno J, Sproson AD, et al. 2019a. Holocene Indian Ocean sea level, Antarctic melting history and past tsunami deposits inferred using sea level reconstructions from the Sri Lankan, Southeastern Indian and Maldivian coasts. *Quat. Sci. Rev.* 206:150–61
Yokoyama Y, Lambeck K, De Deckker P, Esat TM, Webster JM, Nakada M. 2022. Towards solving the missing ice problem and the importance of rigorous model data comparisons. *Nat. Commun.* 13:6261
Yokoyama Y, Purcell A. 2021. On the geophysical processes impacting paleo-sea-level observations. *Geosci. Lett.* 8:13
Yokoyama Y, Yamane M, Nakamura A, Miyairi Y, Horiuchi K, et al. 2019b. In-situ and meteoric ^{10}Be and ^{26}Al measurements: improved preparation and application at the University of Tokyo. *Nucl. Instrum. Methods Phys. Res. B* 455:260–64
You C-F, Lee T, Li Y-H. 1989. The partition of Be between soil and water. *Chem. Geol.* 77:105–18
Ziegler JF. 1999. Stopping of energetic light ions in elemental matter. *J. Appl. Phys.* 85:1249–72